Nanoscale Research Letters

NANO EXPRESS Open Access

Investigation of Band Alignment for Hybrid 2D-MoS_2/3D-β-Ga_2O_3 Heterojunctions with Nitridation

Ya-Wei Huan[1†], Ke Xu[2†], Wen-Jun Liu[1*], Hao Zhang[2], Dmitriy Anatolyevich Golosov[3], Chang-Tai Xia[4], Hong-Yu Yu[5], Xiao-Han Wu[1], Qing-Qing Sun[1] and Shi-Jin Ding[1]

Abstract

Hybrid heterojunctions based on two-dimensional (2D) and conventional three-dimensional (3D) materials provide a promising way toward nanoelectronic devices with engineered features. In this work, we investigated the band alignment of a mixed-dimensional heterojunction composed of transferred MoS_2 on β-Ga_2O_3(2−01) with and without nitridation. The conduction and valence band offsets for unnitrided 2D-MoS_2/3D-β-Ga_2O_3 heterojunction were determined to be respectively 0.43 ± 0.1 and 2.87 ± 0.1 eV. For the nitrided heterojunction, the conduction and valence band offsets were deduced to 0.68 ± 0.1 and 2.62 ± 0.1 eV, respectively. The modified band alignment could result from the dipole formed by charge transfer across the heterojunction interface. The effect of nitridation on the band alignments between group III oxides and transition metal dichalcogenides will supply feasible technical routes for designing their heterojunction-based electronic and optoelectronic devices.

Keywords: Nitridation treatment, Band alignment, Few-layer MoS_2, β-Ga_2O_3

Background

Beta-gallium oxide (β-Ga_2O_3) has attracted considerable interests due to its superior material properties [1, 2]. With ultra-wide bandgap (4.6–4.9 eV), the theoretical breakdown electric field (E_C) is estimated to be around 8 MV/cm [3, 4]. Combined with its high relative dielectric constant (ε) and electron mobility (μ), the Baliga's figure of merit ($\varepsilon\mu E_C^3$) is triple that of GaN or SiC, reducing the conduction loss significantly [1]. In addition, the availability of large bulk single crystals synthesized via melt-growth and epitaxial techniques delivers significant advantages for industrial applications [5, 6]. By far, β-Ga_2O_3 has been well demonstrated in a wide range of electronic applications, including light-emitting diodes, gas sensors, photodetectors, as well as field-effect transistors [7–10]. Very recently, hybrid heterojunctions, i.e., the integration of two-dimensional (2D) materials with three-dimensional (3D) materials, are of particular interest due to the complementary properties of their material systems [11].

To date, diverse 2D layered materials have been stacked on wide bandgap semiconductors to construct hybrid heterojunctions for novel applications with varying functionalities, such as MoS_2/GaN, WSe_2/GaN, MoS_2/SiC, and so on [12–15]. Structurally, the MoS_2 crystal is composed of a Mo atomic layer sandwiched between two sulfur layers, forming a two-dimensional hexagonal trilayer which is bonded to its neighboring layers by weak van der Waals forces [16, 17]. Unlike graphene with a zero bandgap, the thickness-dependent modulation of bandgaps motivated the exploration of MoS_2 in optical and electrical devices [18, 19]. Based on the physics of MoS_2, the density of states of few-layer MoS_2 is three orders of magnitude higher than that of single-layer (SL) MoS_2, leading to high drive currents in the ballistic limit. In this context, few-layer MoS_2 may deliver significant advantages for transistor applications than SL MoS2 [18]. Thus, the integration of MoS_2 with β-Ga_2O_3 is of great interest for combining respective merits of both the established 2D and 3D materials. And the optical and electrical properties for hybrid heterojunctions are

* Correspondence: wjliu@fudan.edu.cn
†Ya-Wei Huan and Ke Xu contributed equally to this work.
[1]State Key Laboratory of ASIC and System, School of Microelectronics, Fudan University, Shanghai 200433, China
Full list of author information is available at the end of the article

inherently dominated by the interfacial energy band alignment. Consequently, it is quite desirable to have tunable band alignments for improving the performance of heterojunction based devices. In this work, we investigated the band alignment of 2D-MoS_2/3D-β-Ga_2O_3 heterojunctions with and without nitridation treatment via X-ray photoelectron spectroscopy (XPS) characterizations and first principles calculations.

Methods

The SiO_2/Si substrate was ultrasonicated with acetone and visopropanol for each 10 min, respectively, followed by rinsing in deionized water and drying with N_2. Few-layer MoS_2 films were grown on the SiO_2/Si substrate by chemical vapor deposition (CVD) using precursors of MoO_3 (0.08 mg, 99%, Alfa Aesar) and S powder (1 g, 99%) [20, 21]. The MoO_3 and S powder were placed into two separate crucibles with a SiO_2/Si substrate in the quartz tube, as shown in Fig. 1a. During the growth process, the quartz tube was held at 800 °C for MoS_2 film growth within 5 min. Figure 1b displays the optical microscopic image of uniform MoS_2 film on SiO_2/Si substrate. After the growth of MoS_2 film, it would be transferred to β-Ga_2O_3 (Tamura Corporation, Japan) substrate via PMMA-assisted method, [22] as sketched in Fig. 1c. During the transfer process, PMMA was first spin-coated on as-grown MoS_2 film as a supporting layer, and then the samples were immersed in KOH solution for etching away the SiO_2 layer. Subsequently, the PMMA layer with MoS_2 film would float on the solution, after which the sample would be rinsed in deionized water for 1 min to remove the residual K^+ and

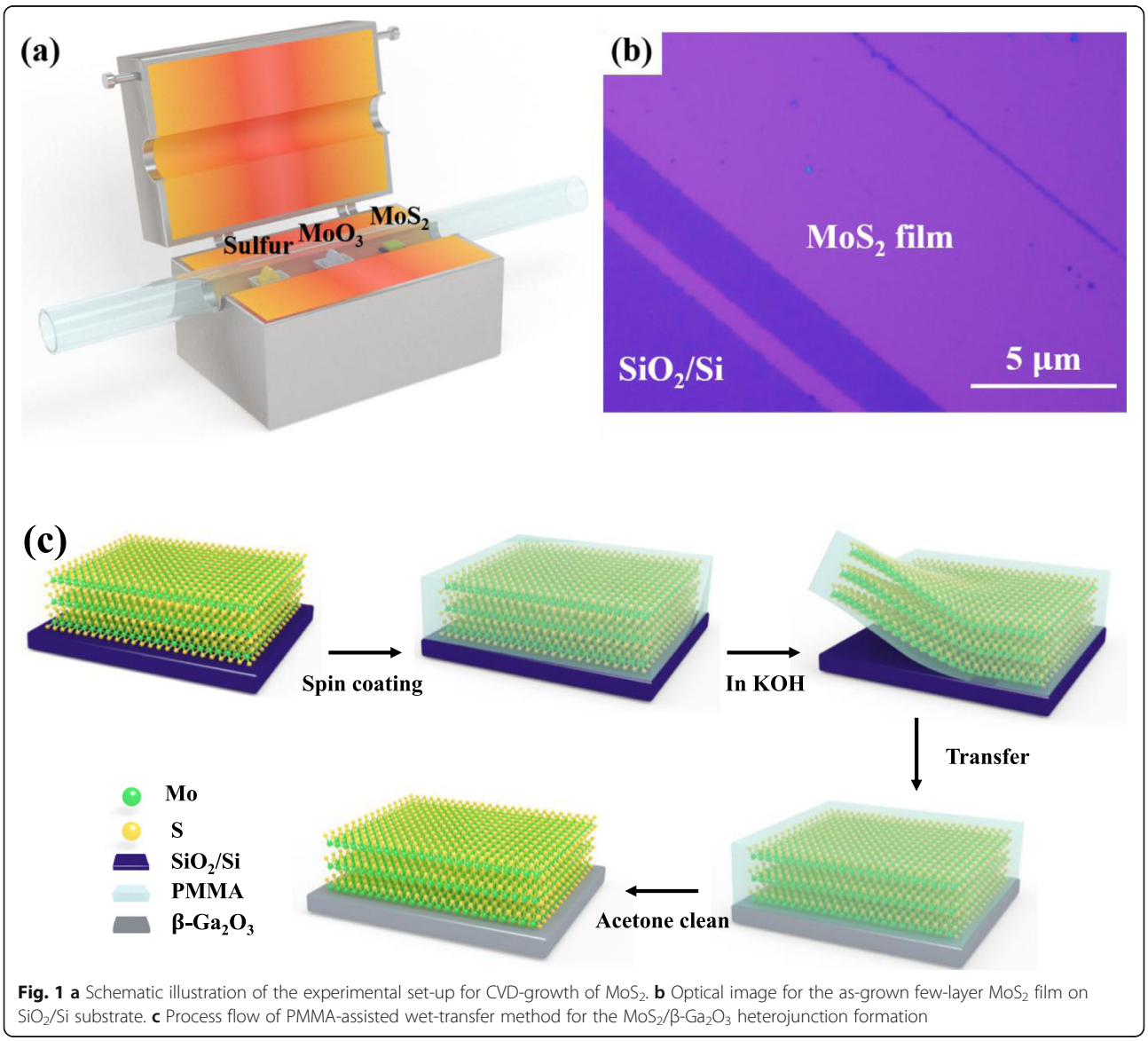

Fig. 1 **a** Schematic illustration of the experimental set-up for CVD-growth of MoS_2. **b** Optical image for the as-grown few-layer MoS_2 film on SiO_2/Si substrate. **c** Process flow of PMMA-assisted wet-transfer method for the MoS_2/β-Ga_2O_3 heterojunction formation

further transferred onto β-Ga_2O_3 substrate. Lastly, the top PMMA layer would be removed away with acetone. For the nitrided MoS_2/β-Ga_2O_3 heterojunction, the nitridation has been implemented on the β-Ga_2O_3 surface with 50s N_2 plasma treatment at a pressure of 3 Pa prior to the MoS_2 transfer. The RF power and N_2 flow rate were 100 W and 80 sccm, respectively. As a result, four samples were prepared for XPS measurements: (1) uncoated β-Ga_2O_3 substrate (bulk β-Ga_2O_3), (2) few-layer MoS_2 film on SiO_2/Si substrate (few-layer MoS_2), (3) transferred MoS_2 film on β-Ga_2O_3 substrate, (4) transferred MoS_2 film on nitrided β-Ga_2O_3 substrate.

Results and Discussions

Raman spectroscopy was employed to investigate the quality of few-layer MoS_2 film as well as to check relevant layer numbers. The Raman spectra of MoS_2 film before and after transfer are presented in Fig. 2, which was characterized by RENISHAW inVia Raman spectroscopy. Two characteristic Raman modes could be observed around 381.91 cm^{-1} and 405.84 cm^{-1}, corresponding to the in-plane (E^1_{2g}) mode and out-of-plane (A_{1g}) mode, respectively [23, 24]. Compared with as-grown MoS_2 film, there is almost no Raman shift in E^1_{2g} and A_{1g} modes after transfer process, indicative of undamaged MoS_2 after transfer process. The peak at 412.99 cm^{-1} after transfer process stems from the β-Ga_2O_3 substrate, in consistent with previous reports [25]. The frequency difference between E^1_{2g} and A_{1g} mode was deduced to be about 23.93 cm^{-1}, designating four layers of few-layer MoS_2 film [26]. Further, as shown in the inset of Fig. 2, the thickness of MoS_2 film was verified to be 3 nm approximately (around four layers) by high-resolution transmission electron microscope (HRTEM), which is in good agreement with our Raman spectra. It can be seen from Fig. 3a that a high intensity peak of N 1 s was detected from the nitride β-Ga_2O_3 substrate, suggesting the presence of nitrogen. Figure 3b shows the SIMS profiles of MoS_2/β-Ga_2O_3 heterojunction with nitridation, where the signals of main components represented by Mo, N, and Ga are plotted against depth. It is observed that the N peak is located at the MoS_2/β-Ga_2O_3 interface, and the N spreading into β-Ga_2O_3 substrate could be contributed by the N injection into the underlying layer during plasma treatment or primary beam bombardments. The higher Ga profile in the MoS_2 layer than β-Ga_2O_3 substrate probably stems from the different ion yield in the different material matrix [27]. Moreover, the tail of Mo in β-Ga_2O_3 could be ascribed to the diffusion or depth resolution problem, which is caused by primary beam bombardment [28].

To obtain the band alignments of MoS_2/β-Ga_2O_3 heterojunctions, XPS measurements with a step of 0.05 eV were carried out on VG ESCALAB 220i-XL system with a monochromatic Al Kα X-ray source (hν = 1486.6 eV). The constant pass energy was set at 20 eV. Additionally, the standard C 1 s (284.8 eV) was used for binding energy (BE) calibration [29]. To evaluate the valence band offset (VBO) at the MoS_2/β-Ga_2O_3 interface, Mo 3d and Ga 3d core levels

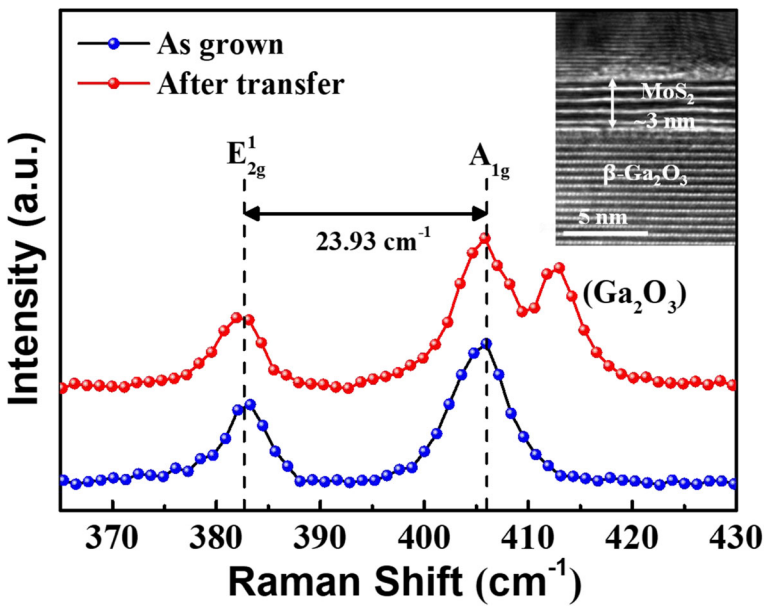

Fig. 2 Raman spectra of as-grown MoS_2 on SiO_2/Si substrate and transferred MoS_2 on β-Ga_2O_3 substrate, respectively. The inset shows cross-section transmission electron microscopy (TEM) image of fabricated MoS_2/β-Ga_2O_3 heterojunction

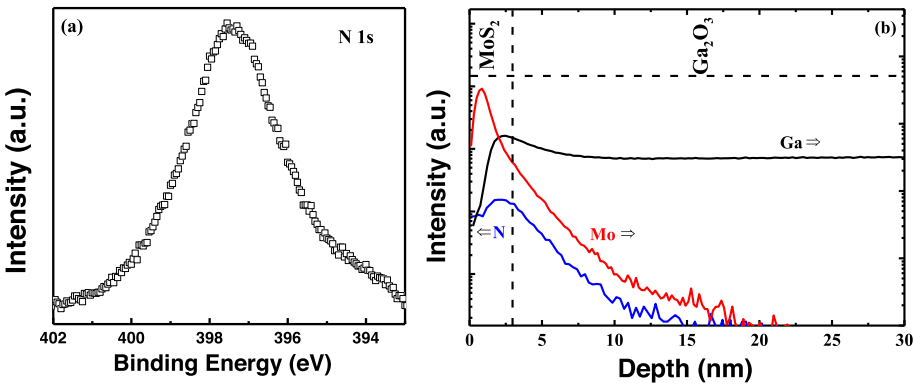

Fig. 3 **a** N 1 s XPS spectrum of β-Ga_2O_3 substrate with surface nitridation. **b** SIMS depth profile of fabricated MoS_2/β-Ga_2O_3 heterojunction

(CLs) were used for few-layer MoS_2 and β-Ga_2O_3 samples, respectively. Figure 4a shows the XPS narrow scan of Mo 3d and valence band spectra from few-layer MoS_2 [30]. The binding energy difference (BED) between CLs of Mo $3d_{5/2}$ and valence band maximum (VBM) for MoS_2 was calculated to be 228.59 ± 0.1 eV. As shown in Fig. 4b, the BE of Ga 3d CL and VBM from few-layer β-Ga_2O_3 were deduced to be 20.25 ± 0.05 and 3.23 ± 0.05 eV, respectively. The corresponding BED was determined to 17.02 ± 0.1 eV, which is well consistent with that reported by Sun et al. [31]. Figure 4c depicts the measured XPS spectra of Mo 3d and Ga 3d CLs for MoS_2/β-Ga_2O_3 heterojunctions with/without nitridation. It is noted that the Mo $3d_{5/2}$ CL shifted from 228.95 ± 0.05 eV for the unnitrided heterojunction toward 229.60 ± 0.05 eV for the nitrided heterojunction while Ga 3d CL shifted from 20.25 ± 0.05 to 20.65 ± 0.05 eV. Based on Kraut' method,[32] the valence band offset (VBO, ΔE_V) of few-layer MoS_2/β-Ga_2O_3 heterojunctions was calculated according to the following equation,

$$\Delta E_V = \left(E^{MoS_2}_{Mo\ 3d_{5/2}} - E^{MoS_2}_{VBM}\right) - \left(E^{Ga_2O_3}_{Ga\ 3d} - E^{Ga_2O_3}_{VBM}\right) - \Delta E_{CL} \quad (1)$$

where $E^{MoS_2}_{Mo\ 3d_{5/2}}$ and $E^{MoS_2}_{VBM}$ are binding energies of Mo $3d_{5/2}$ CL and VBM from MoS_2, $E^{Ga_2O_3}_{Ga\ 3d}$, and $E^{Ga_2O_3}_{VBM}$ are binding energies of Ga 3d CL and VBM from β-Ga_2O_3, $\Delta E_{CL} = (E^{MoS_2}_{Mo\ 3d_{5/2}} - E^{Ga_2O_3}_{Ga\ 3d})$ is the binding energy difference between Mo $3d_{5/2}$ and Ga 3d CLs for MoS_2/β-Ga_2O_3 heterojunctions. Hence, the ΔE_V of MoS_2 on β-Ga_2O_3 substrate with and without N_2 plasma treatment was calculated to be 2.62±0.1 and 2.87 ± 0.1 eV, respectively.

Figure 4d shows the O 1 s CL energy loss spectra of β-Ga_2O_3 substrates with and without nitridation. It is noted that the bandgap keeps unchanged after nitridation treatment with a value of 4.70 ± 0.1 eV. Thus, the conduction band offset can be extracted as follows,

$$\Delta E_C = E_g^{Ga_2O_3} - E_g^{MoS_2} - \Delta E_V \quad (2)$$

where $E_g^{Ga_2O_3}$ and $E_g^{MoS_2}$ are the bandgaps of β-Ga_2O_3 and few-layer MoS_2, respectively. The bandgap of 1.4 ± 0.1 eV for few-layer MoS_2 was used in this work.[34] According to Eq. (2), the ΔE_C between MoS_2 and β-Ga_2O_3 with and without nitridation were deduced to be 0.68 ± 0.1 and 0.43 ± 0.1 eV, respectively. The calculated band diagrams for heterojunctions without/with nitridation are shown in Fig. 5(a) and 5(b), respectively.

Next, the electronic structures of nitrided and unnitrided heterojunctions were further examined through the Vienna ab initio simulation package (VASP) based on density functional theory (DFT) [33–35]. The generalized gradient approximation (GGA) of Perdew-Burke-Ernzerhof (PBE) parameterization was adopted for exchange-correlation function [36, 37]. We used the DFT-D3 dispersion corrections approach to describe the long-distance van der Waals (vdW) interactions [38–40]. The projector augmented wave (PAW) pseudopotential method was used to describe the core-valence interaction with a kinetic energy cutoff of 650 eV for plane wave expansion. We employ a 4 × 4 × 1 G-centered k-mesh for structural relaxation of the unit cell, with the smallest spacing between k-points of 0.04 $Å^{-1}$, which is precise enough by the convergence test with respect to the number of k points. The convergence thresholds are set to 10^{-4} eV for energy differences of the system and 10^{-2} eV $Å^{-1}$ for Hellman-Feynman force. In order to eliminate artificial interactions between two adjacent atomic layers, the thickness of the vacuum layer is set to

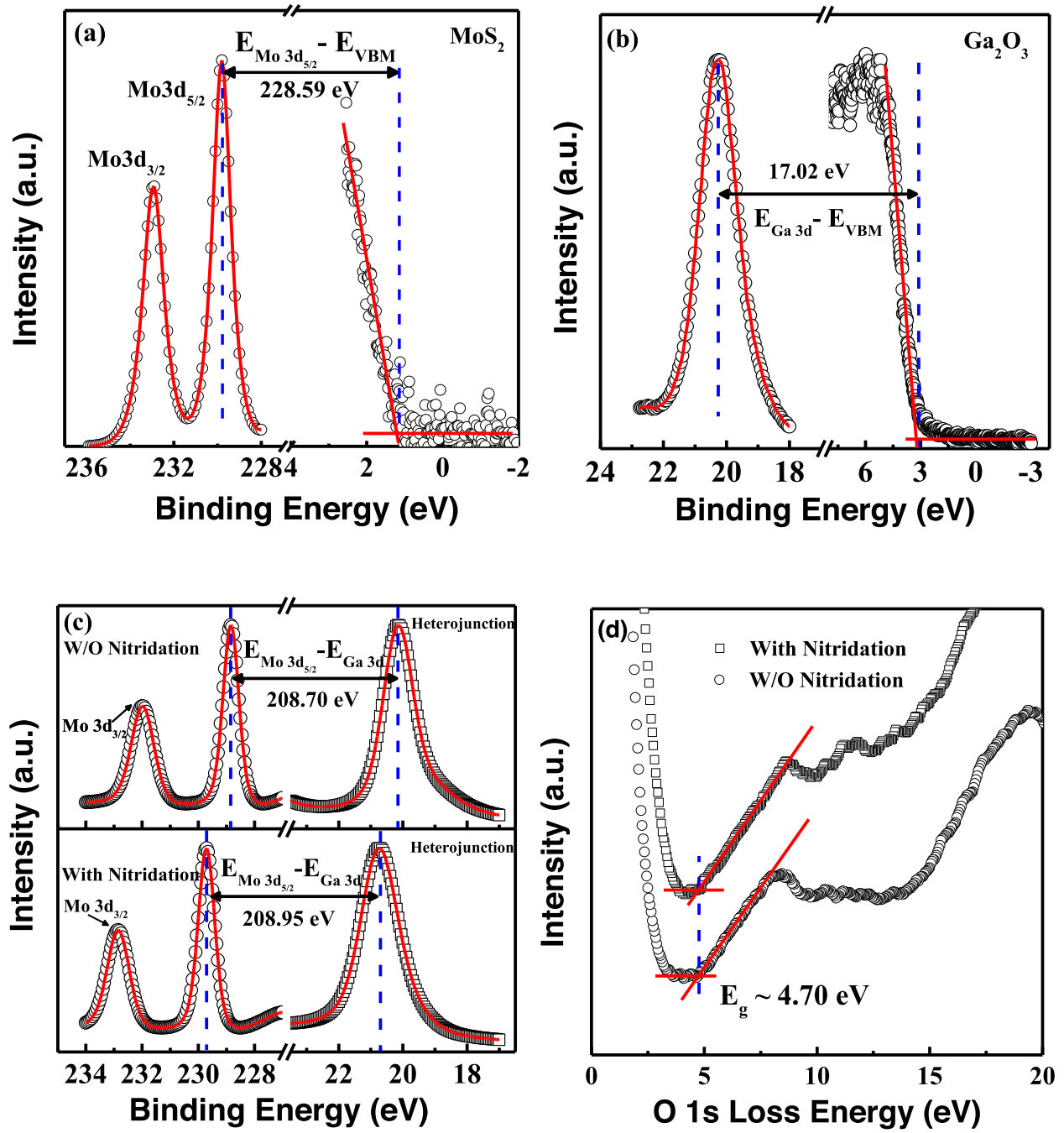

Fig. 4 **a** XPS spectra of Mo 3d CL and valence band from few-layer MoS_2. **b** XPS spectra of Ga 3d CL and valence band from β-Ga_2O_3 substrate. **c** XPS spectra of Mo 3d and Ga 3d CLs for fabricated MoS_2/β-Ga_2O_3 heterojunction with/without surface nitridation. **d** XPS spectra of O 1 s CL energy loss of β-Ga_2O_3 substrate with/without surface nitridation

~ 15 Å. The eigenvalues of the heterojunctions are further verified by the Heyd-Scuseria-Ernzerhof (HSE06) hybrid functional calculations, which improve the precision of eigenvalues via reducing the localization and delocalization errors of PBE and Hartree-Fock (HF) functionals [41]. The mixing ratio is 25% for the short-range HF exchange. The screening parameter is 0.2 $Å^{-1}$.

The MoS_2/β-Ga_2O_3 heterojunctions were constructed as shown in Fig. 6a. The universal binding energy relation (UBER) method, which provides a

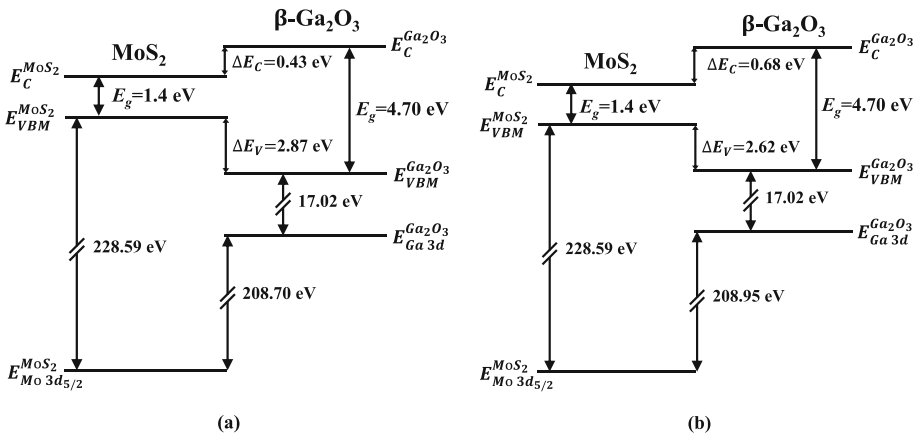

Fig. 5 Band diagrams of MoS_2/β-Ga_2O_3 heterojunction **a** without and **b** with surface nitridation

simple universal form for the relationship between binding energy and atomic separation, [42] was applied to determine the energetically stable structure before electronic structure calculation. Various interlayer distances were considered and the surface adhesion energy W_{ad} for the heterojunctions are shown below,

$$W_{ad} = \frac{E_{Ga_2O_3} + E_{MoS_2} - E_{Ga_2O_3/MoS_2}}{A}$$

where A is the interface area, $E_{Ga_2O_3}$, E_{MoS_2}, and $E_{Ga_2O_3/MoS_2}$ are the total energies of β-Ga_2O_3, monolayer MoS_2 and the MoS_2/β-Ga_2O_3 heterojunction, respectively. Once the W_{ad} reaches a maximum, the optimal interlayer distance will be obtained. After structure optimizations, a nitrogen atom is substitutionally doped in the original MoS_2/β-Ga_2O_3 heterojunction, as shown in Fig. 6b. The concentration of nitrogen in DFT calculation is around 4.17%, which is close to that (3.61%) in experiments. The electronic structures for both nitrided and unnitrided MoS_2/β-Ga_2O_3 heterojunctions were calculated as illustrated in Fig. 6c and d. It was seen that mid-gap states were introduced, which may enhance the charge transfer across the MoS_2/β-Ga_2O_3 interface, and the resulting interface dipole contributed to the measured binding

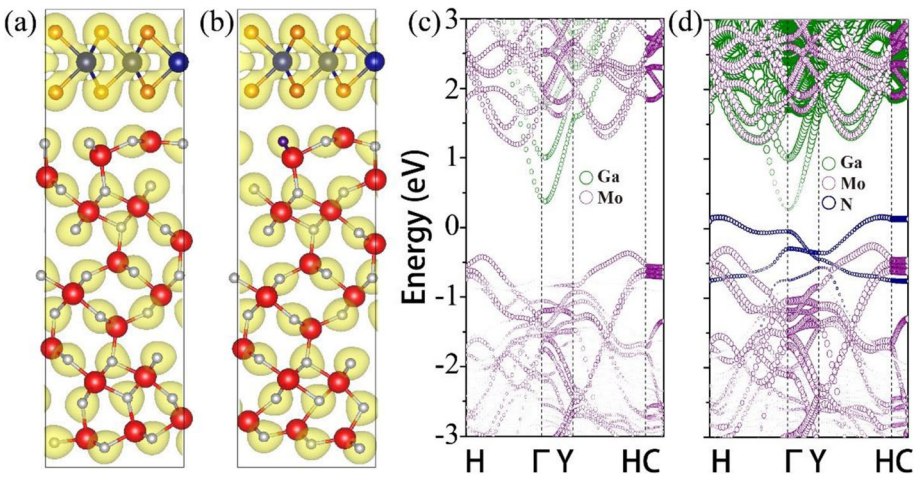

Fig. 6 Atomic structure and charge-density distributions of β-Ga_2O_3-MoS_2 stacked heterostructures **a** without and **b** with nitrogen dopants in a 4 × 4 × 1 supercell from a side view. Ga (O) atoms are in red (gray) and Mo (S) atoms in blue (orange). Band structures of MoS_2/β-Ga_2O_3 heterostructures **c** without and **d** with nitrogen dopants

energy shift. Furthermore, the calculated conduction band offsets ΔE_C ($\Delta E_C = E_{CB}^{MoS_2} - E_{CB}^{Ga_2O_3}$) for undoped- and doped-β-Ga_2O_3/MoS_2 heterojunctions are 0.82 and 1.0 eV respectively, showing the same trend with the experimental results. We have also calculated the eigenvalues of $E_{CB}^{MoS_2}$ and $E_{CB}^{Ga_2O_3}$ using the HSE06 method to further confirm the above conclusion, and find that the corrected ΔE_C are 0.87 and 1.08 eV for undoped- and doped-β-Ga_2O_3/MoS_2 heterojunctions respectively.

Conclusions

In conclusion, respective MoS_2 film has been transferred onto unnitrided and nitride β-Ga_2O_3 for constructing MoS_2/β-Ga_2O_3 heterojunctions. Raman spectroscopy was used to investigate the quality of transferred MoS_2 film, and SIMS study was performed to probe the elemental depth profiles of the MoS_2/β-Ga_2O_3 heterojunction with nitridation. The VBOs were determined to be 2.62 ± 0.1 eV for nitrided MoS_2/β-Ga_2O_3 heterojunction and 2.87 ± 0.1 eV for unnitrided heterojunction by XPS, respectively. The resultant CBOs were deduced to be 0.68 ± 0.1 and 0.43 ± 0.1 eV, which was in the same trends with the DFT calculations. These findings demonstrated that the band offsets can be modified via surface nitridation process. This study offers glorious perspectives on the implementation of designed electronic devices based on 2D/3D vertical heterojunctions.

Abbreviations

β-Ga_2O_3: Beta-gallium oxide; SL: Single-layer; MoS_2: Molybdenum disulfide; XPS: X-ray photoelectron spectroscopy; CBO: Conduction band offset; VBO: Valence band offset; CVD: Chemical vapor deposition; PMMA: Poly(methyl methacrylate); HRTEM: High-resolution transmission electron microscope; SIMS: Secondary ion mass spectrometry; BE: Binding energy; BED: Binding energy difference; CL: Core level; VBM: Valence band maximum; VASP: Vienna ab initio simulation package; DFT: Density functional theory; GGA: Generalized gradient approximation; PBE: Perdew-Burke-Ernzerhof; PAW: Projector augmented wave; UBER: Universal binding energy relation

Acknowledgements

The authors would like to acknowledge the financial support partially by the Key-Area Research and Development Program of GuangDong Province (Grant No. 2019B010128001), National Natural Science Foundation of China (Grant No. 61774041), National Key Technologies Research and Development Program of China (Grant No. 2017YFB0405600), and Shanghai Science and Technology Innovation Program (Grant No.19520711500).

Authors' Contributions

WHY performed the experiments. KX performed the theoretical calculations. WHY and KX contributed equally to this work. WJL and HZ modified the manuscript. DAG, CTX, HYY, XHW, QQS, and SJD helped review and discuss the manuscript. All authors read and approved the final manuscript.

Availability of Data and Materials

The datasets supporting the conclusions of this manuscript are included within the manuscript.

Competing Interests

The authors declare that they have no competing interests.

Author details

[1]State Key Laboratory of ASIC and System, School of Microelectronics, Fudan University, Shanghai 200433, China. [2]Key Laboratory of Micro and Nano Photonic Structures, Department of Optical Science and Engineering, Fudan University, Shanghai 200433, China. [3]Belarusian State University of Informatics and Radioelectronics, P. Brovka street, 6, 220013 Minsk, Belarus. [4]Key Laboratory of Materials for High Power Laser, Shanghai Institute of Optics and Fine Mechanics, Chinese Academy of Sciences, Shanghai 201800, China. [5]Department of Electrical and Electronic Engineering, Southern University of Science and Technology, Shenzhen 518055, China.

Received: 14 July 2019 Accepted: 10 October 2019
Published online: 02 December 2019

References

1. Higashiwaki M, Jessen GH (2018) Guest Editorial: The dawn of gallium oxide microelectronics. Appl Phys Lett 112(6):60401
2. Pearton SJ, Yang JH, Cary P, Ren F, Kim J, Tadjer MA, Mastro M (2018) A review of Ga_2O_3 materials, processing, and devices. Appl Phys Rev 5:11301
3. Mastro MA, Kuramata A, Calkins J, Kim J, Ren F, Pearton SJ (2017) Perspective—opportunities and future directions for Ga_2O_3. ECS J. Solid State Sci. Technol. 6(5):356–359
4. Ma N, Tanen N, Verma A, Guo Z, Luo T, Xing H, Jena D (2016) Intrinsic electron mobility limits in β-Ga_2O_3. Appl Phys Lett 109(21):212101
5. Baldini M, Galazka Z, Wagner G (2017) Recent progress in the growth of β-Ga_2O_3 for power electronics applications. Mat Sci Semicon Proc 78:132–146
6. Higashiwaki M, Kuramata A, Murakami H, Kumagai Y (2017) State-of-the-art technologies of gallium oxide (Ga_2O_3) power devices. J Phys D: Appl Phys 50(33):333002
7. Higashiwaki M, Sasaki K, Murakami H, Kumagai Y, Koukitu A, Kuramata A, Masui T, Yamakoshi S (2016) Recent progress in Ga_2O_3 power devices. Semiconductor Sci Technol 31(3):34001
8. Kan S, Takemoto S, Kaneko K, Takahashi I, Sugimoto M, Shinohe T, Fujita S (2018) Electrical properties of α-Ir_2O_3/α-Ga_2O_3 pn heterojunction diode and band alignment of the heterostructure. Appl Phys Lett 113(21):212104
9. Pilliadugula R, Gopalakrishnan N (2018) Gas sensing performance of GaOOH and β-Ga_2O_3 synthesized by hydrothermal method: a comparison. Mater Res Express 6(2):25027
10. Oshima T, Hashikawa M, Tomizawa S, Miki K, Oishi T, Sasaki K, Kuramata A (2018) β-Ga_2O_3-based metal–oxide–semiconductor photodiodes with HfO_2 as oxide. Appl Phys Express 11(11):112202
11. Jariwala D, Marks TJ, Hersam MC (2017) Mixed-dimensional van der Waals heterostructures. Nat Mater 16(2):170–181
12. Henck H, Ben Aziza Z, Zill O, Pierucci D, Naylor CH, Silly MG, Gogneau N, Oehler F, Collin S, Brault J, Sirotti F, Bertran FO, Le Fèvre P, Berciaud S, Johnson ATC, Lhuillier E, Rault JE, Ouerghi A (2017) Interface dipole and band bending in the hybrid p-n heterojunction MoS_2/GaN(0001). Phys Rev B 96(11):115312
13. Krishnamoorthy S, Lee EW, Lee CH, Zhang Y, Mcculloch WD, Johnson JM, Hwang J, Wu Y, Rajan S (2016) High current density 2D/3D MoS_2/GaN Esaki tunnel diodes. Appl Phys Lett 109(18):183505
14. Tangi M, Mishra P, Tseng C, Ng TK, Hedhili MN, Anjum DH, Alias MS, Wei N, Li L, Ooi BS (2017) Band alignment at GaN/single-layer WSe_2 interface. Acs Appl Mater Inter 9(10):9110–9117
15. Lee EW, Ma L, Nath DN, Lee CH, Arehart A, Wu Y, Rajan S (2014) Growth and electrical characterization of two-dimensional layered MoS_2/SiC heterojunctions. Appl Phys Lett 105(20):203504
16. Eda G, Fujita T, Yamaguchi H, Voiry D, Chen M, Chhowalla M (2012) Coherent atomic and electronic heterostructures of single-layer MoS_2. Acs Nano 6(8):7311–7317
17. Conley HJ, Wang B, Ziegler JI, Haglund RF Jr, Pantelides ST, Bolotin KI (2013) Bandgap engineering of strained monolayer and bilayer MoS_2. Nano Lett 13(8):3626–3630
18. Ganatra R, Zhang Q (2014) Few-layer MoS_2: a promising layered semiconductor. Acs Nano 8(5):4074–4099
19. Ramakrishna Matte H, Gomathi A, Manna AK, Late DJ, Datta R, Pati SK, Rao C (2010) MoS_2 and WS_2 analogues of graphene. Angewandte Chemie International Edition 49(24):4059–4062
20. Zobel A, Boson A, Wilson PM, Muratov DS, Kuznetsov DV, Sinitskii A (2016) Chemical vapour deposition and characterization of uniform bilayer and trilayer MoS_2 crystals. J Mater Chem C 4(47):11081–11087

21. Wong SL, Liu H, Chi D (2016) Recent progress in chemical vapor deposition growth of two-dimensional transition metal dichalcogenides. Prog Cryst Growth Ch 62(3):9–28
22. Ma D, Shi J, Ji Q, Chen K, Yin J, Lin Y, Zhang Y, Liu M, Feng Q, Song X (2015) A universal etching-free transfer of MoS_2 films for applications in photodetectors. Nano Res 8(11):3662–3672
23. Lee C, Yan H, Brus LE, Heinz TF, Hone J, Ryu S (2010) Anomalous lattice vibrations of single- and few-layer MoS_2. Acs Nano 4(5):2695–2700
24. Li H, Zhang Q, Yap CCR, Tay BK, Edwin THT, Olivier A, Baillargeat D (2012) From bulk to monolayer MoS_2: evolution of raman scattering. Adv Funct Mater 22(7):1385–1390
25. Onuma T, Fujioka S, Yamaguchi T, Itoh Y, Higashiwaki M, Sasaki K, Masui T, Honda T (2014) Polarized Raman spectra in β-Ga_2O_3 single crystals. J Cryst Growth 401:330–333
26. Muratore C, Hu JJ, Wang B, Haque MA (2014) Continuous ultra-thin MoS_2 films grown by low-temperature physical vapor deposition. Appl Phys Lett 104(26):261604
27. Deline VR, Katz W, Evans CA Jr, Williams P (1978) Mechanism of the SIMS matrix effect. Appl Phys Lett 33(9):832–835
28. Liu X, He J, Liu Q, Tang D, Jia F, Wen J, Lu Y, Yu W, Zhu D, Liu W, Cao P, Han S, Pan J, He Z, Ang K (2015) Band alignment of HfO_2/multilayer MoS_2 interface determined by x-ray photoelectron spectroscopy: Effect of CHF_3 treatment. Appl Phys Lett 107(10):101601
29. Ebel MF, Ebel H (1974) About the charging effect in X-ray photoelectron spectrometry. J Electron Spectrosc Relat Phenomena 3(3):169–180
30. Chambers SA, Droubay T, Kaspar TC, Gutowski M (2004) Experimental determination of valence band maxima for $SrTiO_3$, TiO_2, and SrO and the associated valence band offsets with Si (001). Journal of Vacuum Science & Technology B: Microelectronics and Nanometer Structures Processing, Measurement, and Phenomena 22(4):2205–2215
31. Sun H, Castanedo CGT, Liu K, Li KH, Guo W, Lin R, Liu X, Li J, Li X (2017) Valence and conduction band offsets of β-Ga_2O_3/AlN heterojunction. Appl Phys Lett 111(16):162105
32. Kraut EA (1980) Precise determination of the valence-band edge in X-ray photoemission spectra: application to measurement of semiconductor interface potentials. Phys Rev Lett 44(24):1620–1623
33. Hafner J (2008) Ab-initio simulations of materials using VASP: density-functional theory and beyond. J Comput Chem 29(13):2044–2078
34. Gui Y, Tang C, Zhou Q, Xu L, Zhao Z, Zhang X (2018) The sensing mechanism of N-doped SWCNTs toward SF_6 decomposition products: a first-principle study. Appl Surf Sci 440:846–852
35. Liu D, Gui Y, Ji C, Tang C, Zhou Q, Li J, Zhang X (2019) Adsorption of SF_6 decomposition components over Pd (111): a density functional theory study. Appl Surf Sci 465:172–179
36. Perdew JP, Burke K, Ernzerhof M (1996) Generalized gradient approximation made simple. Phys Rev Lett 77(18):3865
37. Grimme S (2006) Semiempirical GGA-type density functional constructed with a long-range dispersion correction. J Comput Chem 27(15):1787–1799
38. Wang Y, Gui Y, Ji C, Tang C, Zhou Q, Li J, Zhang X (2018) Adsorption of SF_6 decomposition components on Pt_3-TiO_2 (101) surface: A DFT study. Appl Surf Sci 459:242–248
39. Wei H, Gui Y, Kang J, Wang W, Tang C (2018) A DFT study on the adsorption of H_2S and SO_2 on Ni doped MoS_2 monolayer. Nanomaterials-Basel 8(9):646
40. Xu K, Xu Y, Zhang H, Peng B, Soukoulis CM (2018) Role of anderson rule in determining electronic, optical and transport properties of transition-metal dichalcogenides heterostructure. Phys Chem Chem Phys 20(48)
41. Jochen H, Scuseria GE (2004) Efficient hybrid density functional calculations in solids: assessment of the Heyd-Scuseria-Ernzerhof screened Coulomb hybrid functional. J Chem Phys 121(3):1187–1192
42. Rose JH, Ferrante J, Smith JR (1981) Universal binding energy curves for metals and bimetallic interfaces. Phys Rev Lett 47(9):675

Publisher's Note